THE JOURNAL OF PHYSICAL CHEMISTRY C

Article

pubs.acs.org/JPCC

Understanding Quantum Plasmonics from Time-Dependent Orbital-Free Density Functional Theory

Hongping Xiang, Mingliang Zhang, Xu Zhang, and Gang Lu*

Department of Physics and Astronomy, California State University Northridge, California 91330, United States

Supporting Information

ABSTRACT: Using time-dependent orbital-free density functional theory, we perform quantum mechanical simulations to understand plasmonic responses in sodium nanoparticle dimers and trimers. The electronic structure, optical absorption, electric field enhancement, and photoinduced tunneling current are examined. For dimers, the maximum field enhancement is reached at a gap distance of 6 Å, below which a conductive channel is formed. The tunneling current peaks at the resonant energy of the charge-transfer plasmon (CTP). One such CTP is formed in symmetric linear trimers, and it splits into two in asymmetric linear trimers—one corresponds to a "global" and the other a "local" oscillation as a result of constructive and destructive interferences between the CTPs of the corresponding dimers. The interference leads to "nanofocusing" where the intensity of the "global" mode reaches its maximum while the "local" mode is quenched completely. Similarly, the electric field can be tuned to be localized at one of the two gaps and vanish at the other.

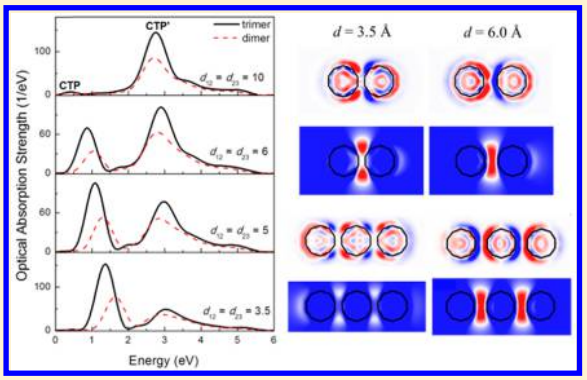

Electromagnetic radiation can excite collective oscillations of conduction electrons in metallic nanoparticles, known as localized surface plasmon resonances (LSPRs). These LSPRs of individual metal nanoparticles not only can be tuned according to their size, shape, composition, and environment,[1−7] but can also be altered through near-field electromagnetic coupling between the neighboring nanoparticles.[8−15] This phenomenon has been widely demonstrated, with the simplest case being a nanoparticle dimer in which two nanoparticles are separated by a small gap.[16−21]

When two nanoparticles are placed at a nanometer distance, their optically driven free electrons couple dynamically across the gap, giving rise to large field enhancements in their junctions.[22−27] These enhancements have been exploited in many applications, such as optical nanoantennas for high-sensitivity chemical and biological sensors,[28,29] surface-enhanced Raman scattering (SERS),[28,30] and higher harmonic light generation,[31,32] to name but a few. Furthermore, coupling multiple nanoparticles together in chainlike structures has also been suggested as an approach to nanoscale optical waveguiding and focusing.[33,34] The rapid advances in this research area are also fueled by theoretical progress, in addition to the experimental explorations. At present, the majority of theoretical studies for the coupled plasmonic systems rely on classical electromagnetic theories,[35−41] and the interfaces between the nanoparticles are often assumed to be abrupt and sharp. While these assumptions are justified for large gap distances, quantum effects start to dominate when the gap distances reach subnanometer scale.[16,20,42−45] Since the classical theories generally fail to capture quantum effects, ranging from electron density spill-out to electron tunneling, they can lead to unphysical predictions, such as diverging field enhancements at small interparticle distances.[46] To rectify the problems, quantum mechanical approaches that fully account for nonlinear and nonlocal effects are essential and can completely change the spectral distribution and the field enhancements predicted by the classical theories.[47−49] There are some recent theoretical efforts to incorporate quantum effects into the classical theories, including the quantum corrected model,[16,50,51] the projected dipole layer model,[48,52] and the extended hydrodynamic model.[47,53] Notwithstanding their usefulness, fully quantum mechanical descriptions based on explicit treatment of ground- and excited-state charge densities are highly desirable and in fact often necessary for reliable predictions. On this regard, time-dependent density functional theory (TDDFT) has been very successful and widely used to capture electron tunneling and screening across the nanojunctions and to yield finite field enhancements at the interfaces.[47,49,54−60] Unfortunately, TDDFT calculations are computationally demanding for even moderately sized plasmonic systems, and as a result, previous TDDFT works have been confined to small nanoparticle dimers.[55,56,58−60] More importantly, many TDDFT calculations have been performed in conjunction with jellium model[46,47,49,54,57,61,62] in order to reduce the computational cost. In the jellium model, the ionic charge density of a nanoparticle is assumed to be uniform, terminating at the nanoparticle surface. This uniform charge density along with the ionic potential are empirical

Received: June 9, 2016

DOI: 10.1021/acs.jpcc.6b05841
J. Phys. Chem. C XXXX, XXX, XXX−XXX

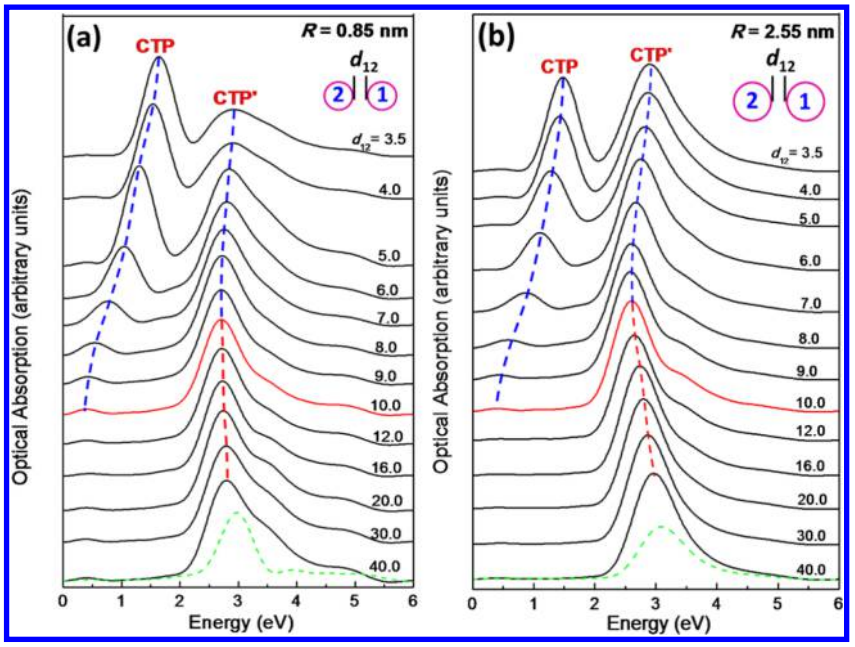

Figure 1. (a and b) Optical absorption spectrum of the dimer with R = 0.85 nm (Na_{55}), and 2.55 nm (Na_{1415}) as a function of the interparticle distance d_{12}. The green dashed curve is the optical spectrum of the isolated particle Na_{55} (left) and Na_{1415} (right).

parameters that need to be adjusted in the simulations to yield correct results. For tunneling across the nanoparticles, special care must be taken to the choice of the termination profile of the ionic potential and to ensuring that the results are converged with respect to this choice.

In this paper, a promising alternative approach based on time-dependent orbital-free density functional theory (TD-OFDFT)[63] is advocated for quantum plasmonics. Compared to TDDFT, TD-OFDFT makes a key additional approximation. Instead of expressing the kinetic energy of noninteracting electrons as Laplacian of single-particle wave functions, one approximates the kinetic energy as a functional of electron density in TD-OFDFT. The kinetic energy consists of two contributions: (1) static kernel terms introduced originally in the orbital-free density functional theory (OFDFT)[64,65] and (2) a dynamic kinetic energy potential term.[63] While the static kernel terms had been developed a long time ago, the dynamic term was developed recently. Given the nature of these approximations, TD-OFDFT is in general more accurate for nearly uniform electron gas, such as Na, and less reliable for localized electrons. However, strides have been made recently to improve the kernel terms in OFDFT with reliable results being obtained for transition metals[66,67] and semiconductors.[68,69] It is thus hoped that such progress would inspire future development of the crucial dynamic term. Since TD-OFDFT depends explicitly on electron density as opposed to single-particle wave functions, the time-consuming procedure of orthonormalization of the wave functions is avoided, leading to linear scaling of computational time versus number of electrons in TD-OFDFT, in contrast to cubic scaling in TDDFT. As a result, TD-OFDFT can treat at least 1 order of magnitude more electrons than the TDDFT counterpart.

Two recent developments are crucial for the success of the TD-OFDFT method. The first is the introduction of the dynamic kinetic energy potential (DKEP) that ensures the correct frequency- and wave-vector-dependent linear response of electron gas in the TD-OFDFT formulation;[63] the second is the construction of ab initio local pseudopotentials[70] for describing the positive charge background more realistically than the jellium model. The orbital-free nature of TD-OFDFT endows it with numerical efficacy to treat many thousands of electrons, well beyond the capability of the standard TDDFT methods. The ab initio local pseudopotentials afford the chemical specificity and atomistic details necessary to understand quantum plasmonics for coupled nanoparticles. The proposed TD-OFDFT method has been employed to examine optical properties of single Na nanoparticles with a considerable success.[71] Herein we show that the same method can be equally successful for coupled nanoparticles, capturing essential quantum effects across the junctions. We first apply the method to Na nanoparticle dimers for which TDDFT and experimental results are available for comparisons. We show that the TD-OFDFT method can provide a more accurate description than the TDDFT jellium model as compared to the experimental results. We then proceed to examine plasmonic responses of Na nanoparticle linear trimers, which has not been attempted quantum mechanically before. Thanks to the TD-OFDFT method, several interesting physical phenomena are revealed for the first time for the trimers with potential applications.

In the TD-OFDFT calculations, a real space grid is used to propagate the charge density in real time under the influence of a time-varying electromagnetic field, which is in the axial direction of the dimers and the linear trimers. The local density approximation[72] for the electron exchange and correlation is used. The ionic potential of Na is described by a local pseudopotential determined from first-principles calculations.[70,71] We have performed a convergence check on the dimensions of the supercell and found that the dimensions of the supercell with 2.5 times the diameter of the Na dimer or trimer were sufficient to eliminate spurious dimer−dimer or trimer−trimer interactions. A uniform mesh grid with a spacing of 0.35 Å was used over which the charge density and potential were calculated. We have verified that the grid spacing of 0.35 Å yielded the converged results as shown in Figure S4 of Supporting Information. The simulation zone in TD-OFDFT,

DOI: 10.1021/acs.jpcc.6b05841
J. Phys. Chem. C XXXX, XXX, XXX−XXX

beyond which the charge density vanishes, was defined by assigning a sphere with a radius of 8 Å around each atom. This choice of the radius was necessary for numerical convergence. Fast Fourier transform was used to calculate the Coulomb potential and convolution integrals in the kinetic energy functional. The linear response calculations were performed by propagating the electron wave packets under a perturbation of an impulse field $E(t) = E_{kick}\delta(t)$.[73] In the real-time propagation, the electronic wave packets were evolved for 7500 steps with a time step of $\Delta t = 0.0015\hbar/\text{eV}$.

We first focus on Na nanoparticle dimers—two identical nanoparticles with a radius R separated by a variable distance d_{12} as shown schematically in Figure 1. Two such dimers are considered—Na_{55} (with 55 electrons) and Na_{1415} (with 1415 electrons), respectively. The corresponding radius of the nanoparticle is R = 0.85 and 2.55 nm, respectively. The nanoparticles are assumed to be of a symmetric icosahedral (I_h) shape, which is experimentally stable.[74] In Figure 1, parts a and b, we display computed optical absorption spectra of the Na dimers as a function of the separation distance d_{12}. Note that d_{12} is the distance between the opposing outmost atomic planes in each icosahedron. As a reference, the corresponding absorption spectra of the isolated Na nanoparticles are also displayed. At large gaps (d_{12} > 10 Å), electron tunneling is negligible and the absorption is dominated by the bonding dipolar plasmon (BDP)—a hybridization between the dipolar plasmon modes of the individual nanoparticles.[54,75] A higher energy shoulder (~5 eV) comprising hybridized bonding quadrupolar plasmon (BQP) is also visible in Figure 1a. The resonant energy of the BDP red-shifts as d_{12} decreases in the range of 10 Å < d_{12} < 40 Å. This red shift along with the formation of BDP and BQP agrees well with previous TDDFT calculations.[46,54] As the gap is reduced below 10 Å, electron tunneling takes place, and eventually a conductive channel is formed across the gap. As a result, two charge-transfer plasmons (CTP and CTP′) appear. The appearance of *two* charge-transfer plasmons and their blue shift with decreasing d_{12} are consistent with the experimental observations[20] and TDDFT calculations with pseudopotentials,[76] hence validating the TD-OFDFT method. By contrast, TDDFT calculations employing the jellium model yielded contradictory results between themselves.[46,54] For example, Zuloaga et al.[46] predicted one charge-transfer plasmon, while Marinica et al.[54] found two for the similar dimers. Note that the only difference between the two TDDFT calculations was those parameters related to the jellium model. Therefore, the choice of the empirical jellium parameters is crucial for an accurate description of plasmonics in the quantum regime. The deficiencies of the jellium model have also been discussed in recent TDDFT studies of Na dimers in the quantum regime.[76,77]

Since an LSPR is a coherent superposition of electron−hole pairs, its energy depends on the following factors in general: (1) the number density of conduction electrons involved in the collective oscillation, (2) the average excitation energy of the electron−hole pairs, and (3) the effective depolarization factor. The optical absorption power at a given frequency is proportional to the induced dipole of the system, which in turn is proportional to the number of electrons involved in the collective oscillation. The intensity of the optical absorption, i.e., the absorption cross section is the ratio of the absorption power to the incident flux, thus is proportional to the number of conduction electrons.

For the dimers with a large gap (d_{12} > 10 Å), there is no electron tunneling or direct charge transfer; the electron number density on each particle is the same as that on the isolated particle. Likewise, the average excitation energy of the dimer remains the same as the single particle. Hence, there is only one absorption peak, i.e., BDP, which originates from the plasmonic oscillation on the individual particles. The red shift of BDP as d_{12} decreases thus solely comes from the electrostatic interaction between the particles. As shown in the Supporting Information, the field produced by the induced dipole on the first particle enhances the external field on the second one, which effectively reduces the depolarization factor of the second particle and its resonant energy. As the gap distance decreases, the field enhancement increases; thus, the resonant energy is red-shifted.

When the gap distance d_{12} is between 7 and 10 Å, electron tunneling takes place. As a result, the BDP transitions to CTP′ and a new CTP forms. We attribute the higher energy CTP′ to the plasmonic oscillation on the individual particles, while the lower energy CTP is attributed to the tunneled electrons oscillating between the two particles. As d_{12} is reduced, the tunneled electron number density increases, and so does the resonant energy of CTP. Hence, the CTP blue-shifts and its intensity increases as d_{12} is reduced. In addition, as the two particles approach each other, their electrostatic interaction energy increases while the average electron excitation energy decreases. As shown in the Supporting Information, the latter dominates the former as d_{12} is reduced; thus, the resonant energy of CTP′ is blue-shifted. The intensity of CTP′ is proportional to the number of conduction electrons on each particle, which decreases as d_{12} is lowered; the intensity of CTP′ thus decreases.

When d_{12} is less than 7 Å, the electronic wave functions from the two particles start to overlap, and a conductive channel is established, allowing electron flow across the gap. For the smallest gap distance d_{12} = 3.5 Å, a chemical bond may be formed between the two outmost Na atoms. In this case, there could be more conduction electrons involved in CTP than CTP′, especially in the smaller particle (R = 0.85 nm). Hence, the intensity of CTP could exceed that of CTP′ as shown in Figure 1.

In Figure 2a, we present the energy dependence of the electron current passing across the gap. Appreciable current is observed only for relatively small gap distances (<7 Å). The tunneling current is peaked at the CTP energy as expected. The blue shift of the current peak tracks the blue shift of CTP energy. In Figure 2b, we display the induced charge density (relative to the equilibrium values) evaluated at two frequencies, $\omega 1$ and $\omega 2$. The charge density was obtained by Fourier transform of the charge density distribution from the time domain to the frequency domain. $\omega 1$ and $\omega 2$ correspond to the plasmon frequency of CTP and CTP′, respectively. As a reference, the charge distribution for the isolated particle is also displayed on the right. For a large gap with d_{12} = 20 Å, the charge density of the dimer at $\omega 2$ resembles that of the single particle, showing the characteristics of LSPR. This is in sharp contrast to the charge density at $\omega 1$, which deviates significantly from that of the single particle. This comparison supports to our assignment of CTP′ as the plasmon on the individual particles. As d_{12} is lowered from 20 to 6 Å, the charge density for the dimer at $\omega 2$ is drastically different from that of the single particle, underlying the transition from BDP to CTP′.

DOI: 10.1021/acs.jpcc.6b05841
J. Phys. Chem. C XXXX, XXX, XXX−XXX

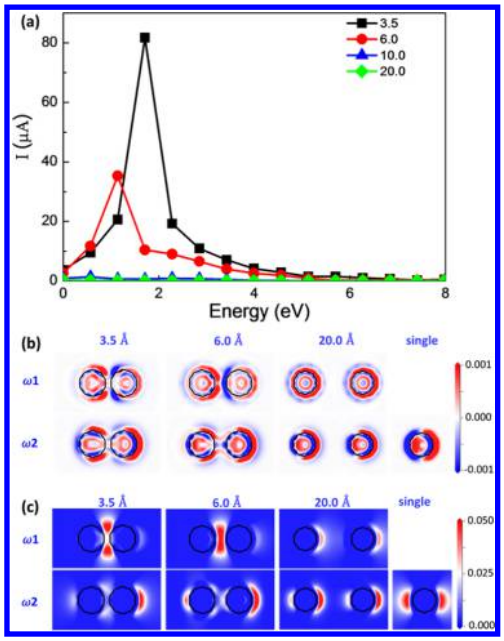

Figure 2. (a) Electron current density across the dimer gap as a function of plasmon energy for d_{12} = 3.5, 6, 10, and 20 Å. (b) The induced charge density (atomic unit) and (c) the electrical field (atomic unit), evaluated at the frequency of $\omega 1$ and $\omega 2$ in response to a horizontal polarization. The magnitude of the charge density and electrical field is color-coded.

Figure 2c shows the electric field distribution of the dimer at $\omega 1$ and $\omega 2$. A field enhancement is observed at the gap for $\omega 1$ as d_{12} decreases from 20 to 6 Å, and reaches the maximum at d_{12} = 6 Å. This field distribution is consistent with the fact that the CTP mode originates from the charge transfer across the gap. The field enhancement starts to decrease as d_{12} reduces to 3.5 Å, at which point a conductive channel is formed and electrons can flow through it, neutralizing the induced charge at the opposite sides of the gap as shown in Figure 2b. By contrast, there is no field enhancement at the gap for $\omega 2$, and the strongest field distribution is found at the ends of the dimer. This is similar to the field distribution of a single particle, again reflecting the fact that CTP′ results from the plasmon on the individual particles. Importantly, we find that the TD-OFDFT calculations eliminate the unphysical singularity of the electric field as predicted by the classical theories.

Having validated the TD-OFDFT method on the dimers, we now apply the method to a linear Na_{55} trimer. As discussed below, interesting phenomena emerge for the trimers that are also expected to exist in other oligomers. We denote d_{12} as the distance between particles 1 and 2, and d_{23} between particles 2 and 3. The optical absorption spectra for four symmetric trimers ($d_{12} = d_{23}$) are shown in Figure 3a. As a comparison, the absorption spectrum for the dimer with the same interparticle distance is also included in the figure. First, we note that two, instead of three, resonant peaks are formed in the symmetric trimers. Second, as compared to the dimers, the lower energy CTP of the trimers is red-shifted while the higher energy CTP′ is blue-shifted. This diverging trend is observed for all gap distances. Third, as the gap decreases, the CTP intensifies while the CTP′ is quenched.

As the gap distance is below 10 Å, there is charge tunneling or transfer across the gap. Similar to the dimers, the higher energy CTP′ is attributed to plasmonic oscillation on the

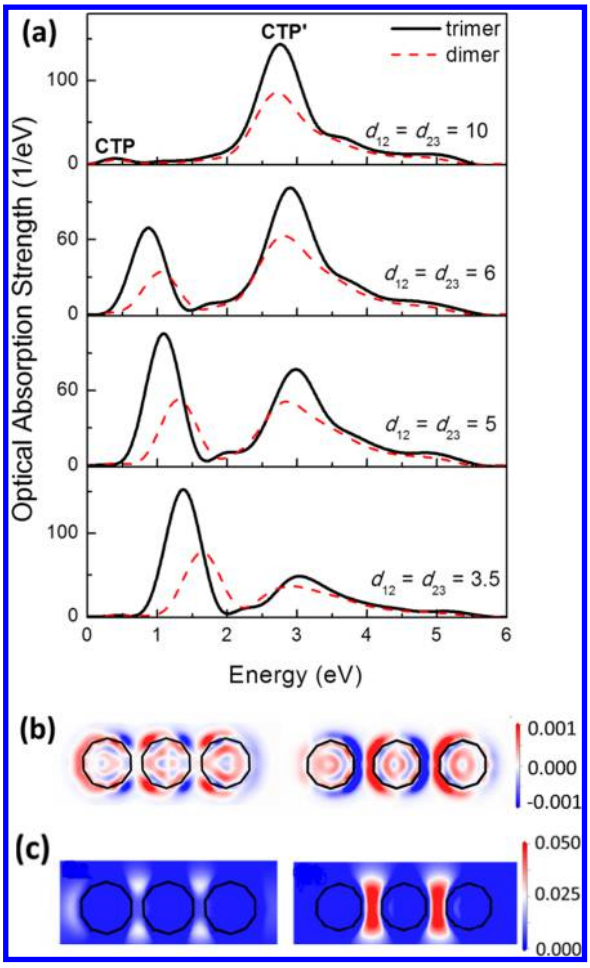

Figure 3. (a) Optical absorption spectrum of the trimer with R = 0.85 nm (Na_{55}) as a function of the interparticle distances ($d_{12} = d_{23}$). (b) The charge density (atomic unit) and (c) electric field (atomic unit) at the CTP frequency for d = 3.5 Å (left) and 6 Å (right) in response to a horizontal polarization. The magnitude of the charge density and electric field is color-coded.

individual particles while the lower energy CTP arises from the tunneled or transferred electrons oscillating among the three particles. What is interesting in this case is that the CTP involves electrons on *all* three particles. More specifically, the CTP represents a "global" oscillation comprising electrons oscillating across the two (or more) gaps in the trimers (or oligomers). Owing to the serial tunneling resistance, the number of conduction electrons involved in the trimer is fewer than that in the dimer; hence, a red shift in CTP relative to the dimer is observed. As fewer electrons are present in CTP, more are available for CTP′, resulting a blue shift relative to the corresponding dimer. In addition, CTP′ exhibits a broadened peak, particularly for smaller gaps owing to the interaction between the particles. As the gap is reduced, the number of tunneled electrons increases while the number of electrons remaining on the particles decreases, leading to a higher intensity of CTP and a lower intensity of CTP′. Finally, the origin of the blue shift for both CTP and CTP′ as the gap decreases is the same as that in the dimers.

In Figure 3b, we present the induced charge density of the trimer relative to the equilibrium values evaluated at the frequency of the CTP. For both gap distances of 3.5 Å (left) and 6 Å (right), the charge density distributions are in-phase

DOI: 10.1021/acs.jpcc.6b05841
J. Phys. Chem. C XXXX, XXX, XXX−XXX

showing the same (blue-to-red) pattern across the two gaps. This is consistent with the "global" plasmonic nature of the CTP. In Figure 3c, we show the electric field distribution of the trimer for the two gap distances. Similar to the dimers, the field enhancement at the gaps is much smaller for d = 3.5 Å (left) as compared to d = 6 Å (right). Moreover, the field distribution is symmetric, which stands in a sharp contrast to the asymmetric trimers as shown below.

We next examine the asymmetric trimers by fixing one of the trimer gaps at d_{12} = 3.5 Å, while reducing the other gap d_{23} from 10 to 3.5 Å. The calculated absorption spectra for the asymmetric trimers are shown in Figure 4a. The CTP modes of the corresponding dimers are also displayed as references. We find that, in addition to the highest energy mode on the individual particles (CTP′), two charge-transfer plasmons appear—termed as CTP1 and CTP2 in the following. We presume that z_{12} electrons are tunneled or transferred from particle 1 to particle 2, and z_{23} electrons are tunneled or transferred from particle 2 to particle 3. Since $d_{12} < d_{23}$, we have $z_{12} > z_{23}$. Thus, there are z_{23} electrons participating in the "global" collective oscillation involving the three particles, while the remaining $z_{12} - z_{23}$ electrons join a "local" collective oscillation involving particles 1 and 2. When d_{23} is large, (e.g., >6 Å), z_{23} is smaller than $(z_{12} - z_{23})$; hence, the "global" oscillation denoted as CTP1 in Figure 4a has a lower energy than the "local" oscillation labeled by CTP2. In this case, the energy of CTP1 and CTP2 is similar to that of CTP for the corresponding dimers as shown in Figure 4a. As d_{23} decreases, z_{23} increases; thus, the absorption intensity of CTP1 increases. At the same time, $(z_{12} - z_{23})$ decreases; hence, the absorption intensity of CTP2 decreases. When d_{23} = 6 Å, the absorption intensity of CTP1 becomes higher than that of CTP2. Finally, as $d_{23} = d_{12}$ = 3.5 Å, $z_{12} - z_{23} = 0$; therefore, the "local" plasmon CTP2 disappears entirely, and we revert to the symmetric trimer case.

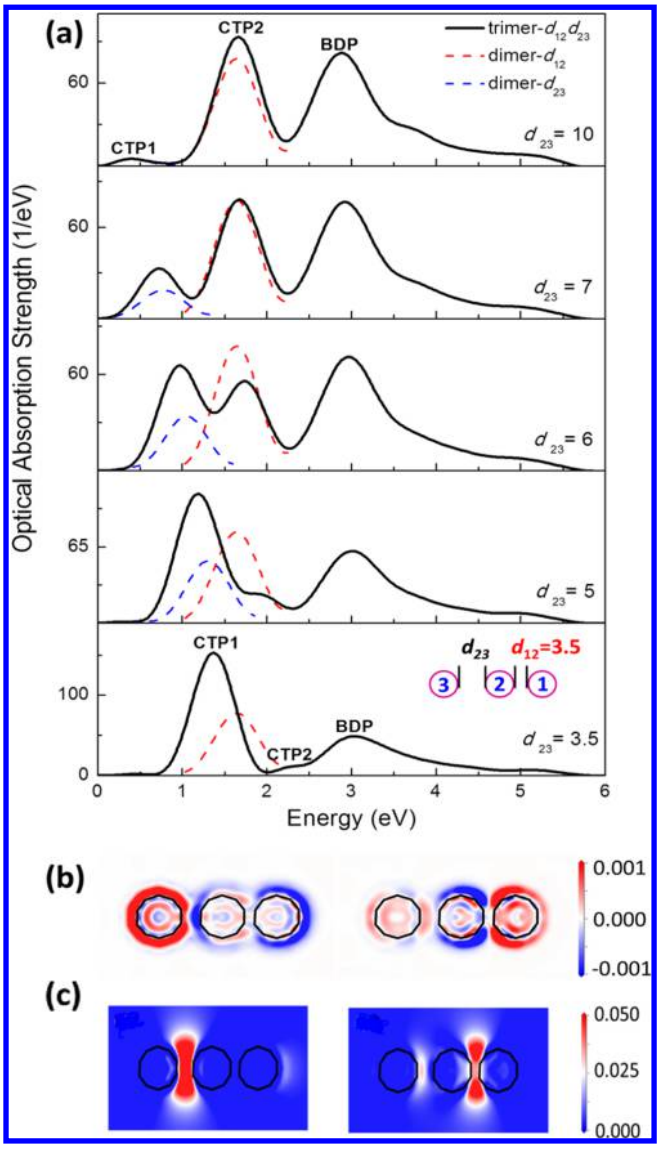

Figure 4. (a) Optical absorption of the trimer with R = 0.85 nm (Na_{55}) as a function of the interparticle distance d_{23}. The optical absorption of the corresponding dimers (dimer-d_{12} and dimer-d_{23}) are also displayed with d_{12} = 3.5 Å (red dashed curve) and d_{23} = 5, 6, 7, and 10 Å (blue dashed curve). (b) The charge density and (c) electric field in atomic unit of the trimer (d_{12} = 3.5 Å and d_{23} = 6 Å) corresponding to CTP1 (left) and CTP2 (right) in response to a horizontal polarization. The magnitude of the charge density and electrical field is color-coded.

To understand the physics further, we plot the induced charge density corresponding to CTP1 and CTP2 for d_{23} = 6 Å in Figure 4b. For CTP1, the plasmon oscillation involves all three particles: particle 3 on the left gains electrons while particles 1 and 2 lose electrons. The charge transfer from particle 2 to 3 is clearly visible. For CTP2, the plasmon oscillation involves the particles 1 and 2 only, with the charge transfer between them. The similar phenomenon is observed in the electric field distribution shown in Figure 4c. For CTP1, the field enhancement occurs at the two ends of the trimer and the gap between the particles 2 and 3. For CTP2, the field enhancement is only present at the gap between the particles 1 and 2. These results are consistent with our interpretation that CTP1 corresponds to the "global" oscillation while CTP2 is the "local" oscillation.

The following physical picture emerges from the analysis of the trimers. One can consider the appearance of CTP1 and CTP2 as the result of constructive and destructive interferences between the charge-transfer plasmons of the corresponding dimers, analogous to Fano resonance often observed in coupled plasmonic nanostructures.[22,78] The constructive interference gives rise to the "global" plasmon oscillation with a lower resonant energy and an increased optical adsorption intensity; the destructive interference leads to the "local" plasmon oscillation with a higher resonant energy and a decreased adsorption intensity. The contrast in the intensity manifests the strongest in the symmetric trimers where CTP1 reaches its maximum intensity while CTP2 quenches completely. In this case, the intensity of CTP1 *doubles* that of the corresponding dimer CTP. This "focusing" effect is also observed in the spatial distribution of the electric field. As shown in Figure 4c, the electric field can be selectively tuned to be localized at either gap, while the electric field at the other gap vanishes. Our results are similar to an earlier work which demonstrated that the self-similar chain of metallic nanospheres could be used as an efficient nanolens to develop a nanofocus or "hottest spot" in the gap.[34] In addition, the disappearance of a plasmonic mode due to the increase of the symmetry in the trimeric plasmonic molecules has also been observed previously.[36] However, there is a crucial difference between the present and the previous results. In the previous works, the coupling between the particles is of electrostatic nature and the relevant

DOI: 10.1021/acs.jpcc.6b05841
J. Phys. Chem. C XXXX, XXX, XXX−XXX

plasmons are of BDP-type. The underlying physics is thus classical, and the classical theory was in fact employed to interpret the results. The present work on the other hand is based on quantum plasmonics, and the relevant plasmons are CTPs. The interference between the CTPs are of quantum nature, and the quantum mechanical TD-OFDFT was used to obtain the results. In comparison to BDPs, CTPs are expected to have lower energy loss and higher transmission efficiencies. We also note that the trimers offer novel physics that cannot be extrapolated from the dimers. On the other hand, the same interference phenomena observed in the trimers could also occur in other oligomers such as tetramers, pentamers, etc. One can thus exploit the interference to gain spatial and temporal control of localized electromagnetic hot spots in coupled plasmonic nanostructures with potential applications in nano-antennas, plasmonic sensors, waveguides, and active meta-materials.

In conclusion, we have performed quantum mechanical TD-OFDFT calculations to understand quantum plasmonics of Na nanoparticle dimers and trimers. The electronic structure, optical absorption, electric field enhancement, and photo-induced tunnel current are examined. Two plasmonic peaks appear in the adsorption spectra of the dimers, consistent with the experimental observations for small gap distances. The field enhancement reaches its maximum at the gap distance of 6 Å, below which a conductive channel is formed and electrons can flow through it. Two plasmonic modes are also observed for the symmetric trimers, with the lower energy CTP representing the "global" oscillation across the three particles and the higher energy CTP′ corresponding to the oscillation on the individual particles. For the asymmetric trimers, the CTP splits into two modes, CTP1 and CTP2, resulting from the constructive and destructive interference between the charge-transfer plasmons of the corresponding dimers, respectively. CTP1 involves the "global" oscillation across the three particles, while CTP2 corresponds to the "local" oscillation between the two nearest-neighbor particles 1 and 2. As d_{23} decreases, CTP1 intensifies while CTP2 is quenched. When $d_{23} = d_{12}$, CTP1 reaches its maximum intensity while CTP2 disappears completely. Similarly, the electric field can be selectively tuned to be localized at either gap.

■ ASSOCIATED CONTENT

Supporting Information

The Supporting Information is available free of charge on the ACS Publications website at DOI: 10.1021/acs.jpcc.6b05841.

Additional discussion and figures concerning the electrostatic interaction between two spheres, interaction of an electron in sphere 1 with sphere 2, and the on-sphere number density $n_s(d_{12})$ of electrons in a dimer (PDF)

■ AUTHOR INFORMATION

Corresponding Author

*E-mail: ganglu@csun.edu.

Notes

The authors declare no competing financial interest.

■ ACKNOWLEDGMENTS

The work was support by the Office of Naval Research (N0014-15-1-2092) and NSF (DMR-1205734).

■ REFERENCES

(1) Kelly, K. L.; Coronado, E.; Zhao, L. L.; Schatz, G. C. *J. Phys. Chem. B* **2003**, *107*, 668.
(2) Jin, R. C.; Cao, Y. C.; Hao, E. C.; Metraux, G. S.; Schatz, G. C.; Mirkin, C. A. *Nature* **2003**, *425*, 487.
(3) Mock, J. J.; Barbic, M.; Smith, D. R.; Schultz, D. A.; Schultz, S. *J. Chem. Phys.* **2002**, *116*, 6755.
(4) de Heer, W. A. *Rev. Mod. Phys.* **1993**, *65*, 611.
(5) Meiwes-Broer, K. H. *Eur. Phys. J. D* **2007**, *45*, 399.
(6) Knight, W. D.; de Heer, W. A.; Saunders, W. A. *Z. Phys. D: At., Mol. Clusters* **1986**, *3*, 109.
(7) Cohen, M. L.; Chou, M. Y.; Knight, W. D.; Deheer, W. A. *J. Phys. Chem.* **1987**, *91*, 3141.
(8) Ward, D. R.; Huser, F.; Pauly, F.; Cuevas, J. C.; Natelson, D. *Nat. Nanotechnol.* **2010**, *5*, 732.
(9) Schuller, J. A.; Barnard, E. S.; Cai, W. S.; Jun, Y. C.; White, J. S.; Brongersma, M. L. *Nat. Mater.* **2010**, *9*, 193.
(10) Le Ru, E. C.; Etchegoin, P. G. *Chem. Phys. Lett.* **2004**, *396*, 393.
(11) Lim, D. K.; Jeon, K. S.; Hwang, J. H.; Kim, H.; Kwon, S.; Suh, Y. D.; Nam, J. M. *Nat. Nanotechnol.* **2011**, *6*, 452.
(12) Alonso-Gonzalez, P.; Albella, P.; Schnell, M.; Chen, J.; Huth, F.; Garcia-Etxarri, A.; Casanova, F.; Golmar, F.; Arzubiaga, L.; Hueso, L. E.; Aizpurua, J.; Hillenbrand, R. *Nat. Commun.* **2012**, *3*, 684.
(13) Zhang, J.; Fu, Y.; Chowdhury, M. H.; Lakowicz, J. R. *Nano Lett.* **2007**, *7*, 2101.
(14) Zhang, Z. L.; Yang, P. F.; Xu, H. X.; Zheng, H. R. *J. Appl. Phys.* **2013**, *113*, 033102.
(15) Lee, H.; Kim, G. H.; Lee, J. H.; Kim, N. H.; Nam, J. M.; Suh, Y. D. *Nano Lett.* **2015**, *15*, 4628.
(16) Savage, K. J.; Hawkeye, M. M.; Esteban, R.; Borisov, A. G.; Aizpurua, J.; Baumberg, J. J. *Nature* **2012**, *491*, 574.
(17) Chang, W. S.; Willingham, B. A.; Slaughter, L. S.; Khanal, B. P.; Vigderman, L.; Zubarev, E. R.; Link, S. *Proc. Natl. Acad. Sci. U. S. A.* **2011**, *108*, 19879.
(18) Halas, N. J.; Lal, S.; Chang, W. S.; Link, S.; Nordlander, P. *Chem. Rev.* **2011**, *111*, 3913.
(19) Rechberger, W.; Hohenau, A.; Leitner, A.; Krenn, J. R.; Lamprecht, B.; Aussenegg, F. R. *Opt. Commun.* **2003**, *220*, 137.
(20) Scholl, J. A.; Garcia-Etxarri, A.; Koh, A. L.; Dionne, J. A. *Nano Lett.* **2013**, *13*, 564.
(21) Saito, S.; Akaishi, Y.; Klar, H.; Nakaichimaeda, S.; Schmid, E. W.; Spitz, G. *Z. Phys. A: At. Nucl.* **1985**, *320*, 399−404.
(22) Zhou, X.; Deeb, C.; Kostcheev, S.; Wiederrecht, G. P.; Adam, P.-M.; Béal, J.; Plain, J.; Gosztola, D. J.; Grand, J.; Félidj, N.; Wang, H.; Vial, A.; Bachelot, R. *ACS Photonics* **2015**, *2*, 121.
(23) Yang, L.; Wang, H.; Fang, Y.; Li, Z. *ACS Nano* **2016**, *10*, 1580.
(24) Troparevsky, M. C.; Zhao, K.; Xiao, D.; Zhang, Z.; Eguiluz, A. G. *Nano Lett.* **2009**, *9*, 4452.
(25) Thijssen, R.; Kippenberg, T. J.; Polman, A.; Verhagen, E. *Nano Lett.* **2015**, *15*, 3971.
(26) Talley, C. E.; Jackson, J. B.; Oubre, C.; Grady, N. K.; Hollars, C. W.; Lane, S. M.; Huser, T. R.; Nordlander, P.; Halas, N. J. *Nano Lett.* **2005**, *5*, 1569.
(27) Sheikholeslami, S. N.; Garcia-Etxarri, A.; Dionne, J. A. *Nano Lett.* **2011**, *11*, 3927.
(28) Xu, H. X.; Bjerneld, E. J.; Kall, M.; Borjesson, L. *Phys. Rev. Lett.* **1999**, *83*, 4357.
(29) Castro, A.; Marques, M. A. L.; Varsano, D.; Sottile, F.; Rubio, A. *C. R. Phys.* **2009**, *10*, 469.
(30) Jiang, J.; Bosnick, K.; Maillard, M.; Brus, L. *J. Phys. Chem. B* **2003**, *107*, 9964.
(31) Ko, K. D.; Kumar, A.; Fung, K. H.; Ambekar, R.; Liu, G. L.; Fang, N. X.; Toussaint, K. C. *Nano Lett.* **2011**, *11*, 61.
(32) Kim, S.; Jin, J. H.; Kim, Y. J.; Park, I. Y.; Kim, Y.; Kim, S. W. *Nature* **2008**, *453*, 757.
(33) Maier, S. A.; Kik, P. G.; Atwater, H. A.; Meltzer, S.; Harel, E.; Koel, B. E.; Requicha, A. A. G. *Nat. Mater.* **2003**, *2*, 229.
(34) Li, K. R.; Stockman, M. I.; Bergman, D. J. *Phys. Rev. Lett.* **2003**, *91*, 227402.

DOI: 10.1021/acs.jpcc.6b05841
J. Phys. Chem. C XXXX, XXX, XXX−XXX

(35) Bao, K.; Mirin, N. A.; Nordlander, P. *Appl. Phys. A: Mater. Sci. Process.* **2010**, *100*, 333.
(36) Chuntonov, L.; Haran, G. *J. Phys. Chem. C* **2011**, *115*, 19488.
(37) Clarkson, J. P.; Winans, J.; Fauchet, P. M. *Opt. Mater. Express* **2011**, *1*, 970.
(38) Ershov, A. E.; Gavrilyuk, A. P.; Karpov, S. V.; Semina, P. N. *Chin. Phys. B* **2015**, *24*, 047804.
(39) Jain, P. K.; El-Sayed, M. A. *J. Phys. Chem. C* **2008**, *112*, 4954.
(40) Osberg, K. D.; Harris, N.; Ozel, T.; Ku, J. C.; Schatz, G. C.; Mirkin, C. A. *Nano Lett.* **2014**, *14*, 6949.
(41) Lermé, J. *J. Phys. Chem. C* **2015**, *119*, 21087.
(42) Tame, M. S.; McEnery, K. R.; Ozdemir, S. K.; Lee, J.; Maier, S. A.; Kim, M. S. *Nat. Phys.* **2013**, *9*, 329.
(43) Arielly, R.; Ofarim, A.; Noy, G.; Selzer, Y. *Nano Lett.* **2011**, *11*, 2968.
(44) Tan, S. F.; Wu, L.; Yang, J. K. W.; Bai, P.; Bosman, M.; Nijhuis, C. A. *Science* **2014**, *343*, 1496.
(45) Zhu, W. Q.; Crozier, K. B. *Nat. Commun.* **2014**, *5*, 5228.
(46) Zuloaga, J.; Prodan, E.; Nordlander, P. *Nano Lett.* **2009**, *9*, 887.
(47) Teperik, T. V.; Nordlander, P.; Aizpurua, J.; Borisov, A. G. *Opt. Express* **2013**, *21*, 27306.
(48) Yan, W.; Wubs, M.; Asger Mortensen, N. *Phys. Rev. Lett.* **2015**, *115*, 137403.
(49) Kulkarni, V.; Manjavacas, A. *ACS Photonics* **2015**, *2*, 987.
(50) Esteban, R.; Borisov, A. G.; Nordlander, P.; Aizpurua, J. *Nat. Commun.* **2012**, *3*, 825.
(51) Scholl, J. A.; Garcia-Etxarri, A.; Aguirregabiria, G.; Esteban, R.; Narayan, T. C.; Koh, A. L.; Aizpurua, J.; Dionne, J. A. *ACS Nano* **2016**, *10*, 1346.
(52) Toscano, G.; Straubel, J.; Kwiatkowski, A.; Rockstuhl, C.; Evers, F.; Xu, H.; Mortensen, N. A.; Wubs, M. *Nat. Commun.* **2015**, *6*, 7132.
(53) David, C.; Garcia de Abajo, F. J. *ACS Nano* **2014**, *8*, 9558.
(54) Marinica, D. C.; Kazansky, A. K.; Nordlander, P.; Aizpurua, J.; Borisov, A. G. *Nano Lett.* **2012**, *12*, 1333.
(55) Yin, H. F.; Zhang, H. *Appl. Phys. Lett.* **2012**, *101*, 061906.
(56) Barbry, M.; Koval, P.; Marchesin, F.; Esteban, R.; Borisov, A. G.; Aizpurua, J.; Sanchez-Portal, D. *Nano Lett.* **2015**, *15*, 3410.
(57) Andersen, K.; Jensen, K. L.; Mortensen, N. A.; Thygesen, K. S. *Phys. Rev. B: Condens. Matter Mater. Phys.* **2013**, *87*, 235433.
(58) Zhang, K.; Zhang, H. *J. Phys. Chem. C* **2014**, *118*, 635.
(59) Yan, J.; Yuan, Z.; Gao, S. W. *Phys. Rev. Lett.* **2007**, *98*, 216602.
(60) Song, P.; Meng, S.; Nordlander, P.; Gao, S. *Phys. Rev. B: Condens. Matter Mater. Phys.* **2012**, *86*, 121410.
(61) Liebsch, A. *Phys. Rev. B: Condens. Matter Mater. Phys.* **1987**, *36*, 7378.
(62) Brack, M. *Rev. Mod. Phys.* **1993**, *65*, 677.
(63) Neuhauser, D.; Pistinner, S.; Coomar, A.; Zhang, X.; Lu, G. *J. Chem. Phys.* **2011**, *134*, 144101.
(64) Wang, L. W.; Teter, M. P. *Phys. Rev. B: Condens. Matter Mater. Phys.* **1992**, *45*, 13196.
(65) Wang, Y. A.; Govind, N.; Carter, E. A. *Phys. Rev. B: Condens. Matter Mater. Phys.* **1999**, *60*, 16350.
(66) Ke, Y. Q.; Libisch, F.; Xia, J. C.; Wang, L. W.; Carter, E. A. *Phys. Rev. Lett.* **2013**, *111*, 066402.
(67) Huang, C.; Carter, E. A. *Phys. Rev. B: Condens. Matter Mater. Phys.* **2012**, *85*, 045126.
(68) Huang, C.; Carter, E. A. *Phys. Rev. B: Condens. Matter Mater. Phys.* **2010**, *81*, 045206.
(69) Shin, I.; Carter, E. A. *J. Chem. Phys.* **2014**, *140*, 18A531.
(70) Huang, C.; Carter, E. A. *Phys. Chem. Chem. Phys.* **2008**, *10*, 7109.
(71) Xiang, H. P.; Zhang, X.; Neuhauser, D.; Lu, G. *J. Phys. Chem. Lett.* **2014**, *5*, 1163.
(72) Ceperley, D. M.; Alder, B. J. *Phys. Rev. Lett.* **1980**, *45*, 566.
(73) Yabana, K.; Bertsch, G. F. *Phys. Rev. B: Condens. Matter Mater. Phys.* **1996**, *54*, 4484.
(74) Peng, S.; McMahon, J. M.; Schatz, G. C.; Gray, S. K.; Sun, Y. G. *Proc. Natl. Acad. Sci. U. S. A.* **2010**, *107*, 14530.
(75) Prodan, E.; Radloff, C.; Halas, N. J.; Nordlander, P. *Science* **2003**, *302*, 419.
(76) Varas, A.; Garcia-Gonzalez, P.; Garcia-Vidal, F. J.; Rubio, A. *J. Phys. Chem. Lett.* **2015**, *6*, 1891.
(77) Zhang, P.; Feist, J.; Rubio, A.; Garcia-Gonzalez, P.; Garcia-Vidal, F. J. *Phys. Rev. B: Condens. Matter Mater. Phys.* **2014**, *90*, 161407.
(78) Luk'yanchuk, B.; Zheludev, N. I.; Maier, S. A.; Halas, N. J.; Nordlander, P.; Giessen, H.; Chong, C. T. *Nat. Mater.* **2010**, *9*, 707.

DOI: 10.1021/acs.jpcc.6b05841
J. Phys. Chem. C XXXX, XXX, XXX−XXX